ADVANCED MATERIALS
www.advmat.de

Materials Views
www.MaterialsViews.com

Carrier-Density Control of the $SrTiO_3$ (001) Surface 2D Electron Gas studied by ARPES

Siobhan McKeown Walker, Flavio Yair Bruno, Zhiming Wang, Alberto de la Torre, Sara Riccó, Anna Tamai, Timur K. Kim, Moritz Hoesch, Ming Shi, Mohammad Saeed Bahramy, Phil D. C. King, and Felix Baumberger*

Combining the tunability of semiconductor heterostructures with the rich properties of correlated electron systems is a central goal in materials science. The 2D electron gas (2DEG) observed at the $LaAlO_3/SrTiO_3$ (LAO/STO) interface[1] emerged as a particularly promising model system in this regard since it combines high mobility with properties such as gate-tunable superconductivity that cannot be realized in conventional semiconductor heterostructures or bulk correlated electron systems.[2–5] The interface 2DEG resides solely in STO and can be stabilized in different ways. These include interfacing STO with other crystalline insulating materials such as spinel Al_2O_3 or perovskite $GdTiO_3$,[6,7] deposition of amorphous overlayers,[8–10] and electrolyte gating.[11] A similar 2DEG has also been observed on the bare surface of STO following irradiation with UV light.[12–14] Irrespective of the method by which the 2DEG is created, the electronic properties of the system are governed by carriers doped into the titanium 3d t_{2g} bands of STO close to the interface or surface.

Control of the 2DEG density has been achieved at the LAO/STO interface by electrostatic gating and by growing samples at different temperatures.[3,15] Subsequent electronic transport experiments have established the thermodynamic phase diagram of the 2DEG as a function of carrier density and provided evidence for a complex electronic structure with multiple orbitally polarized sub-bands,[3,16,17] qualitatively consistent with first-principles electronic structure calculations.[18] While there is strong indirect evidence for this picture,[19] direct measurements of the 2DEG band structure proved difficult. Quantum oscillation measurements at the LAO/STO interface were only successful in the low carrier density regime and are intrinsically restricted to the Fermi energy.[20–22] Angle-resolved photoemission (ARPES) experiments can provide direct momentum space resolution over the entire occupied bandwidth. However, ARPES experiments on buried interfaces require high excitation energies limiting the resolution and sensitivity of the measurements. Consequently, to date only a small subset of the predicted ladder of quantum well states could be resolved on the LAO/STO interface.[23,24] A clearer picture of the 2DEG electronic structure can be obtained from ARPES experiments on the bare surface of STO.[12,25,26] However, these experiments have so far been restricted to a single carrier density largely because the mechanism by which the 2DEG develops in the bare STO(001) surface under UV-light irradiation remained unclear.

Here, we study this mechanism and show that we can create and fully deplete the 2DEG by alternate in situ exposure of the surface to light and small doses of oxygen. This demonstrates that the 2DEG is an electron accumulation layer screening positively charged oxygen vacancy (OV) defects that are created in the surface by irradiating the sample with photons of appropriate energy. We establish that OVs are created via Ti 3p core-hole Auger decay. This channel is only active when photons of $h\nu > 38$ eV are used enabling us to study the electronic structure of the 2DEG by ARPES at intermediate carrier densities by employing either photons below this threshold energy, or by simultaneous irradiation and oxygen exposure.

All experiments shown in the following have been performed with lightly La-doped STO. This results in a residual bulk conductivity that facilitates photoemission experiments but has no measurable influence on the 2DEG electronic structure.[25] **Figure 1**a shows the electronic structure of a 2DEG with saturated bandwidth at the (001) surface of STO measured with a photon energy of 52 eV at a temperature of 10 K. Consistent with earlier experimental studies, we find that the 2DEG bandwidth develops gradually under the light and eventually saturates near 250 meV. The observation of multiple orbitally polarized sub-bands has been interpreted as a consequence of quantum confinement due to band bending

S. McKeown Walker, Dr. F. Y. Bruno, A. de la Torre, S. Riccó, Dr. A. Tamai, Prof. F. Baumberger
Department of Quantum Matter Physics
University of Geneva
24 Quai Ernest-Ansermet, 1211 Geneva, Switzerland
E-mail: flavio.bruno@unige.ch
Dr. Z. Wang, Dr. M. Shi, Prof. F. Baumberger
Swiss Light Source
Paul Scherrer Institute
5232 Villigen, Switzerland
Dr. T. K. Kim, Dr. M. Hoesch
Diamond Light Source
Harwell Campus
Didcot OX11 0DE, UK
Dr. M. S. Bahramy
Quantum-Phase Electronics Center
Department of Applied Physics
University of Tokyo
113-8656 Tokyo, Japan
Dr. M. S. Bahramy
RIKEN Center for Emergent Matter Science
351-0198 Wako, Japan
Dr. P. D. C. King, Prof. F. Baumberger
SUPA School of Physics and Astronomy
University of St Andrews
KY16 9SS St Andrews, UK

DOI: 10.1002/adma.201501556

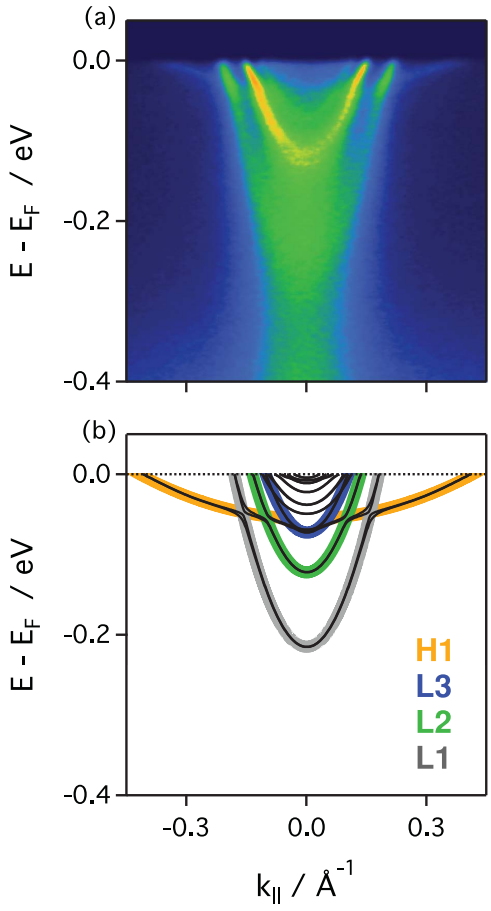

Figure 1. Electronic structure of the 2D electron gas in $SrTiO_3$(001). a) Energy momentum dispersion plot measured in the second Brillouin zone. Measurements shown are the sum of data taken with s- and p-polarized light at 52 eV photon energy and $T = 10$ K. b) Tight binding supercell calculations (black). The three light bands (L1, L2, L3) and the heavy band (H1) resolved in the ARPES measurement are marked in gray, green, blue, and orange, respectively. L1, L2, and L3 have predominantly *xy*-orbital character and H1 has predominantly *xz*/*yz*-orbital character.

near the surface.[12,25] This picture is confirmed by the tight-binding supercell calculations following ref.[26] shown in Figure 1b, which reproduces the three light sub-bands (gray, green, and blue lines) and the heavy sub-band (orange line) that are resolved by the ARPES measurement. The three light sub-bands have predominately *xy*-orbital character and form three concentric circular Fermi surface (FS) sheets. The heavy sub-band belongs to a pair with primarily *xz*/*yz*-orbital character forming two elliptical Fermi surface sheets with their long axes oriented along k_y and k_x, respectively.[26] To estimate the carrier density of the 2DEG, we count the 2D Luttinger volume n_{2D} of the first light sub-band and the two equivalent heavy sub-bands. These criteria give $n_{2D} = 1.9 \times 10^{14}$ cm^{-2} for Figure 1a and will be adopted in the remainder of the manuscript. We note that n_{2D} determined in this way excludes contributions from any small FS sheets of low bandwidth that are not resolved in some of our experiments and thus underestimates the carrier density. From a comparison to self-consistent tight-binding supercell calculations,[26] we estimate that n_{2D} represents approximately 70% of the total sheet carrier density $n_{2D\text{-total}}$ (see Figure S1a, Supporting Information).

To establish that oxygen vacancies lie at the origin of the STO(001) surface 2DEG, we performed a three-step experiment as shown in **Figure 2**a–c. First, we irradiate the surface with photons of 52 eV in order to obtain the fully developed 2DEG shown in Figure 2a.[12] Second, we stop the photon flux and expose the surface to 0.5 Langmuir of O_2. This fully depletes the 2DEG, as is evident from Figure 2b. Finally, we irradiated the sample for a second time with 52 eV photons and observe, as shown in Figure 2c, that the 2DEG has redeveloped. The entirety of the experiment was performed at 10 K without moving the sample or photon beam and all data in Figure 2 were measured with 28 eV photons. This experiment confirms that the 2DEG is a quantum confined accumulation layer of electrons at the surface of STO that screens positive charge resulting from light-induced defects; that the 2DEG is depleted by exposure to oxygen identifies these defects as light-induced oxygen vacancies.

Figure 2d–f shows angle-integrated valence band spectra corresponding to Figure 2a–c, respectively. The valence band leading edge midpoint (VB LEM) is indicated by a cross in each spectrum, and its position with respect to the Fermi level (E_F) is summarized in Figure 2g together with the 2DEG total bandwidth. The clear downward shift of the valence band on irradiated samples indicates a downward bending of the conduction band at the surface. The simultaneous observation of spectral weight at the Fermi level demonstrates that the 2DEG originates from band bending in $SrTiO_3$, as is the case in interface 2DEGs. We note, however, that the shift of the VB LEM is only a qualitative measure of the surface band bending, since it represents an average of the local potential over a few unit cells rather than the exact potential at the surface. In the remainder of the manuscript, we show that doped carriers fill Ti-derived 3d bands, discuss the main mechanism for the creation of oxygen vacancies at the surface, and finally illustrate how this knowledge can be used in order to stabilize different carrier densities in the 2DEG.

In **Figure 3**a,b, we present X-ray photoemission spectroscopy (XPS) measurements of the STO core levels O 1s and Ti 2p respectively, taken at a single position on the sample surface and with photon energy $h\nu = 650$ eV. The XPS measurements are from a pristine as-cleaved surface (gray), after sufficient irradiation with 52 eV light to saturate the 2DEG bandwidth (green), and following oxygen exposure where the 2DEG is fully depleted again (blue). From Figure 3a, we determine that the integrated intensity of the O 1s peak is reduced to approximately 90% of the original value after UV irradiation and largely recovers after exposure to 0.4 L of O_2 (2.6×10^{-9} mbar oxygen partial pressure for 200 s). These observations directly confirm the existence of OVs at the irradiated surface. Moreover, they suggest a remarkable reactivity of vacancies for the dissociation of molecular oxygen offering a possible new route to enhancing the catalytic activity of $SrTiO_3$. That such a low dose of oxygen is sufficient to fully quench the OVs further indicates that they lie in the top few unit cells of the surface, which is plausible given the low temperature of our experiment where vacancy diffusion is negligible. Therefore, to estimate the number of OV per 2D unit cell we assume that they are located either in

ADVANCED MATERIALS
www.advmat.de

www.MaterialsViews.com

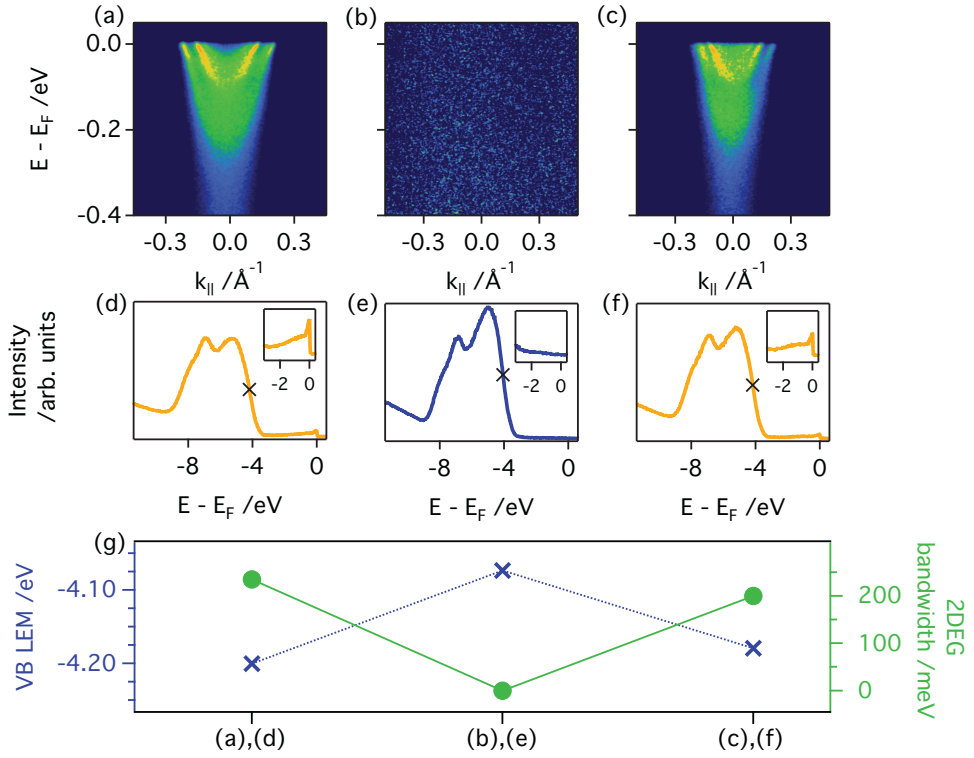

Figure 2. The effect of oxygen on the 2DEG and valence band of the STO(001) surface. a) Dispersion plot of the high density STO(001) surface 2DEG after initial irradiation with 52 eV photons. b,c) The 2DEG disappears after in situ exposure to 0.5 Langmuir of O_2 and reappears following further irradiation with 52 eV photons. d–f) Angle integrated valence band spectra corresponding to the states in (a–c). The magnified insets show the intensity at the Fermi level. The valence band leading edge midpoint (VB LEM) is marked by a cross. g) VB LEM and 2DEG bandwidth that correspond to the states shown in (a–c) and (d–f). All data were measured in the second Brillouin zone with 28 eV, s-polarized light.

the topmost TiO_2 layer or equally distributed over the top TiO_2 and SrO layers. Both of these configurations are found to have a low formation energy in a recent density functional theory study and are stable at low temperature.[27] Accounting for the exponential attenuation of the photoelectron signal from subsurface layers using an inelastic mean free path of 5.5 Å, these models correspond to OV densities of ≈0.53 and ≈0.62 per 2D unit cell on a surface that we measure by ARPES to have $n_{2D\text{-}total} \approx 0.36$ per 2D unit cell. This shows that a substantial fraction of the nominally two excess electrons per OV remain localized on the vacancy and do not contribute to the itinerant carrier density, consistent with recent theoretical studies.[27–29]

The mixed character of OVs is also reflected in the Ti 2p XPS spectra. On surfaces supporting a saturated 2DEG (green spectrum in Figure 3b), we find a clear transfer of spectral weight toward a shoulder on the low binding energy side that can be

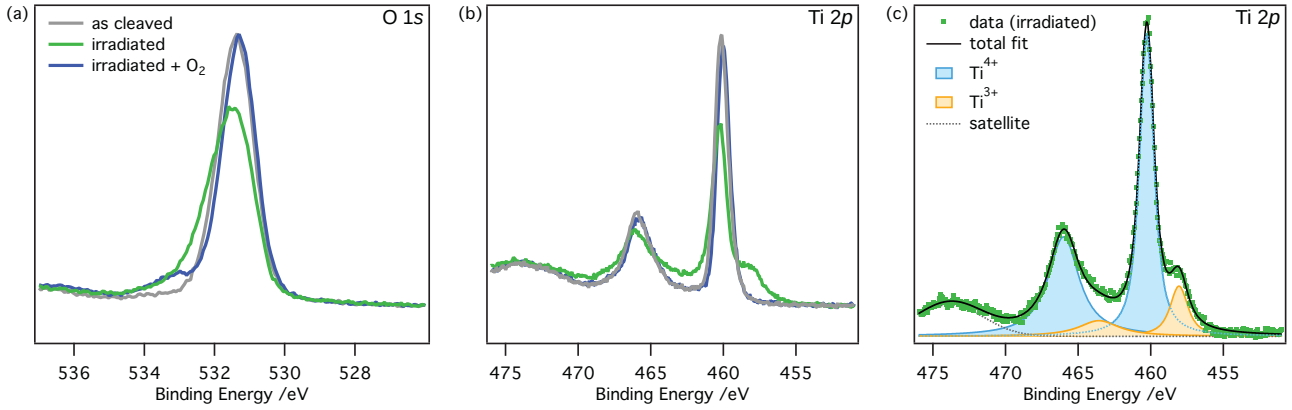

Figure 3. Core level spectroscopy. a,b) X-ray photoemission spectra of oxygen 1s and titanium 2p core levels on the (gray) as-cleaved, (green) irradiated, and (blue) oxygen exposed (0.4 Langmuir) STO(001) surface. The spectra are normalized to the background on the low binding energy side of the peaks. c) Fit to the spin–orbit split $Ti2p_{1/2}$ and $Ti2p_{3/2}$ peaks of the irradiated surface. The Ti 3+ and 4+ peaks are shown in orange and blue shading, respectively.

attributed to Ti^{3+} ions and is also observed at the interface of both crystalline and amorphous LAO layers with STO.[8,30–32] Fitting the XPS spectrum with four Lorentzians convolved with a Gaussian representing the spin–orbit split Ti^{3+} (shaded orange) and Ti^{4+} (shaded blue) peaks, as shown in Figure 3c, we find a ratio of Ti^{3+}/Ti^{4+} sites of ≈20%, averaged over the probing depth. In order to compare this ratio to the Ti^{3+} signal expected from the itinerant t_{2g} carriers in the 2DEG, one needs to model their depth distribution. Assuming a charge density profile as obtained from the tight-binding supercell calculations for a saturated 2DEG with $n_{2D\text{-}total} \approx 0.4$ (see Figure S1b, Supporting Information), we estimate that ≈40% of the Ti^{3+} signal arises from itinerant carriers in the Ti t_{2g} shell. The full experimental Ti^{3+} signal can only be reproduced with solely itinerant carriers by assuming an unphysically narrow charge distribution, where almost all carriers are localized on the topmost TiO_2 layer. This leads us to conclude that Ti^{3+} sites corresponding to electrons localized on or near OVs are present in the system in addition to the Ti^{3+} sites resulting from the itinerant carriers that form the 2DEG. This is consistent with the findings from our O 1s XPS data and might arise from correlation effects or the preferential occupation of localized Ti e_g states in subsurface vacancies as discussed in recent theoretical studies.[27–29]

In **Figure 4**, we show the evolution of the valence band leading edge midpoint as a function of irradiation time measured at two different photon energies: 52 eV (solid symbols) and 26 eV (open symbols). The total shift is a qualitative measure of the direction and relative magnitude of the band bending as discussed previously (see Figure 2d–g). The VB LEM shifts away from the Fermi level as the surface is irradiated which indicates a downward band bending. This shift is small for ≈2400 s irradiation with 26 eV light (open circles) leading to a 2DEG bandwidth <50 meV. A saturated 2DEG with ≈250 meV bandwidth is only obtained after further exposure of the same area for comparable time with 52 eV photons, which results in a large shift of the VB LEM. It is clear from these experiments that the rate at which the VB LEM shifts, and accordingly the rate of oxygen vacancy creation, depends on the photon energy with which the surface is irradiated. This is consistent with the observation of a threshold energy for oxygen vacancy creation by stimulated O^+ desorption in maximal valence oxides first described by Knotek and Feibelman for TiO_2.[33] In this model, the incident photon creates a Ti 3p core hole which is subsequently filled with electrons from neighboring O 2p orbitals via an interatomic Auger process.[34,35] Simple Auger events remove only two electrons from the O^{2-} ion, but in some cases after a double Auger process three electrons can be removed resulting in O^+. The Coulomb repulsion from the surrounding Ti^{4+} in the lattice favors desorption of the ionized oxygen atoms, thus creating oxygen vacancies. The photon energy necessary to create a Ti 3p core hole in STO is ≈38 eV, explaining the much more efficient creation of oxygen vacancies when the surface is irradiated using photon energies above this threshold.

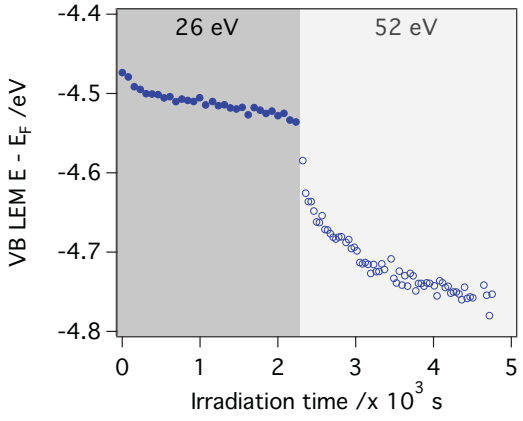

Figure 4. Evidence for oxygen vacancy creation by core hole Auger decay. Valence band leading edge midpoint as a function of irradiation time at $h\nu = 26$ (solid symbols) and 52 eV (open symbols). All points were measured consecutively at the same sample position.

Understanding the mechanism by which the 2DEG develops allows unprecedented control of the carrier densities accessible to ARPES experiments, presenting a new opportunity to trace the evolution of the electronic structure. It is possible to proceed in at least two different ways. First, we can lower the carrier density of a fully developed 2DEG by exposing the surface to low O_2 doses and subsequently probe the band structure with photon energies below the Ti 3p threshold. Alternatively, ARPES experiments can be performed at photon energies above this threshold but in the presence of a low O_2 background pressure. The first approach is illustrated in **Figure 5**a,b where the band dispersion is studied with a photon energy of 28 eV after exposing the surface to 0.1 and 0.2 Langmuir O_2, respectively. We are able to obtain high quality data of these intermediate density states because at this photon energy the carrier density barely varies on the timescale of the experiment. The second alternative is illustrated in Figure 5c,d where the dispersion plots were taken with a photon energy of 52 eV and at an O_2 partial pressure of 6.5×10^{-10} and 1.3×10^{-9} mbar of O_2, respectively. The oxygen vacancies created by the UV light are filled with increased efficiency at higher O_2 partial pressure and the resulting dynamic equilibrium stabilizes different 2DEG carrier densities as has been shown for anatase TiO_2.[36]

Using both methods and collecting data from different samples, we have investigated the evolution of the 2DEG sub-band bandwidth as a function of the carrier density. The results are summarized in Figure 5e, where we plot the energies of the first three light sub-bands and the first heavy sub-band shown schematically in Figure 1b. From the good agreement with single parameter linear fits, we conclude that all sub-band energies are approximately proportional to the carrier density. This behavior is a hallmark of confinement in an asymmetric quantum well and agrees with numerical calculations for different amounts of surface band bending as shown in Figure S2 (Supporting Information). It is also fully consistent with quantum oscillation measurements in STO 2DEGs that observed multiple sub-bands down to very low carrier densities and a splitting of the two lowest lying sub-bands that increases from ≈1 to ≈60 meV when the density increases from 0.7×10^{13} to 8.7×10^{13} cm^{-2}.[7,22]

In summary, we have shown that it is possible to create and fully deplete the 2DEG found at the (001) surface of STO by alternate in situ exposure to light and small O_2 doses demonstrating that oxygen vacancies are responsible for its appearance. We explain the photon-stimulated O desorption process based

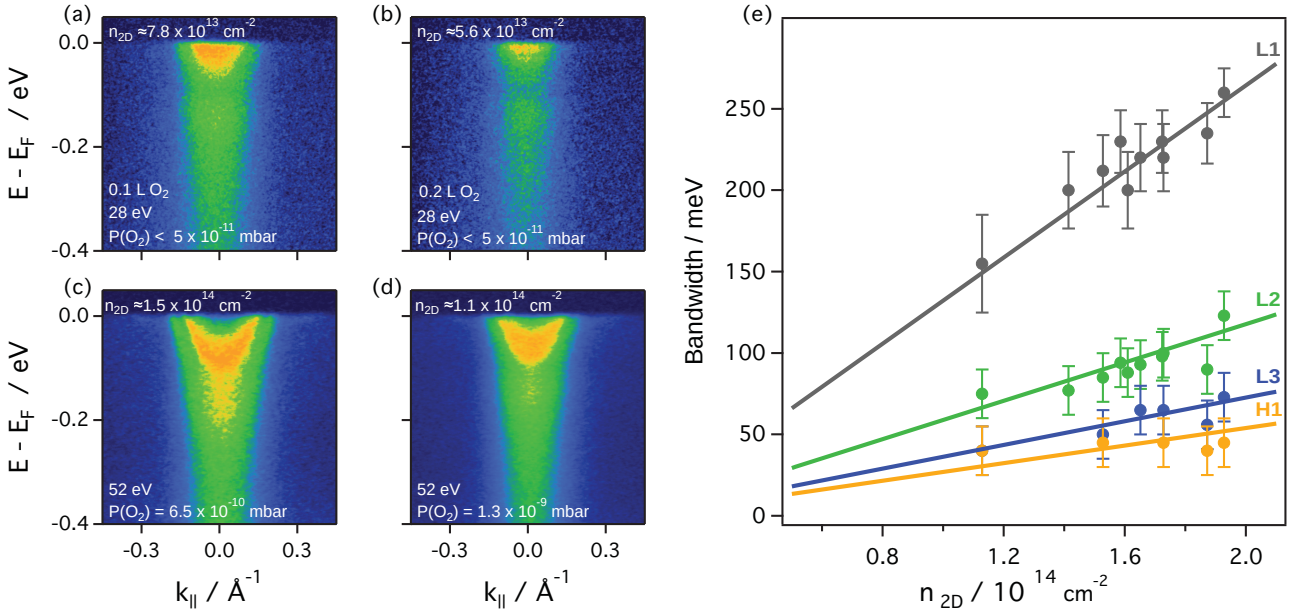

Figure 5. Control of the STO(001) surface 2DEG density. a,b) Dispersion plot measured with 28 eV photons on a surface that initially supported a saturated 2DEG and was subsequently exposed to 0.1 and 0.2 Langmuir O_2. c,d) Dispersion plots measured with 52 eV photons in an oxygen partial pressure of 5×10^{-10} and 2×10^{-9} mbar, respectively. e) Occupied bandwidth as a function of carrier density for the first three light sub-bands (L1, L2, L3) and the first heavy sub-band (H1) indicated in gray, green, blue, and orange, respectively.

on the Ti 3p core hole Auger decay, which is active at photon energies above ≈38 eV. In exploiting this knowledge, we achieve a new level of control of the OV density on the surface of STO, which allows us to establish the evolution of the sub-band bandwidth as a function of carrier density in the 2DEG. The observed variations provide strong support for an interpretation of the 2DEG electronic structure in terms of quantum confinement.

Experimental Section

Experimental Details: La-$SrTiO_3$ substrates with 0.075 wt% La from crystal base were fractured in situ at temperatures <30 K. ARPES measurements were performed at the I05 beamline of the Diamond Light Source and the SIS beamline of the Swiss Light Source. Photon energies between 26 and 140 eV were used with s-, p- and circularly polarized light. XPS measurements were performed at the I05 beamline of the Diamond Light Source at a photon energy of 650 eV with p-polarized light. Samples were measured at temperatures between 6 and 20 K. Results were reproduced on multiple samples.

Supporting Information

Supporting Information is available from the Wiley Online Library or from the author.

Acknowledgements

The authors gratefully acknowledge discussions with Milan Radovic, Nick Plumb, Alex Fête, and Thomas Greber. This work was supported by the Swiss National Science Foundation (200021-146995). P.D.C.K. was supported by the UK-EPSRC EP/I031014/1 and the Royal Society. M.S.B. was partly supported by Grant-in-Aid for Scientific Research (S) (No. 24224009) from the Ministry of Education, Culture, Sports, Science and Technology (MEXT) of Japan. The authors acknowledge Diamond Light Source for time in beamline I05 under proposals SI11741 and SI9837. Open-access data underpinning this publication can be accessed at http://dx.doi.org/10.17630/BA52D718-319E-447A-B517-351C5AF72831.
Note: Figure 1 was updated on July 8, 2015, after initial publication online.

Received: April 1, 2015
Revised: April 29, 2015
Published online: May 22, 2015

[1] A. Ohtomo, H. Y. Hwang, *Nature* **2004**, *427*, 423.
[2] N. Reyren, S. Thiel, A. D. Caviglia, L. F. Kourkoutis, G. Hammerl, C. Richter, C. W. Schneider, T. Kopp, A.-S. Rüetschi, D. Jaccard, M. Gabay, D. A. Muller, J.-M. Triscone, J. Mannhart, *Science* **2007**, *317*, 1196.
[3] A. D. Caviglia, S. Gariglio, N. Reyren, D. Jaccard, T. Schneider, M. Gabay, S. Thiel, G. Hammerl, J. Mannhart, J.-M. Triscone, *Nature* **2008**, *456*, 624.
[4] M. Ben Shalom, M. Sachs, D. Rakhmilevitch, A. Palevski, Y. Dagan, *Phys. Rev. Lett.* **2010**, *104*, 126802.
[5] C. Richter, H. Boschker, W. Dietsche, E. Fillis-Tsirakis, R. Jany, F. Loder, L. F. Kourkoutis, D. A. Muller, J. R. Kirtley, C. W. Schneider, J. Mannhart, *Nature* **2013**, *502*, 528.
[6] Y. Z. Chen, N. Bovet, F. Trier, D. V. Christensen, F. M. Qu, N. H. Andersen, T. Kasama, W. Zhang, R. Giraud, J. Dufouleur, T. S. Jespersen, J. R. Sun, A. Smith, J. Nygård, L. Lu, B. Büchner, B. G. Shen, S. Linderoth, N. Pryds, *Nat. Commun.* **2013**, *4*, 1371.
[7] P. Moetakef, D. G. Ouellette, J. R. Williams, S. James Allen, L. Balents, D. Goldhaber-Gordon, S. Stemmer, *Appl. Phys. Lett.* **2012**, *101*, 151604.

[8] Y. Chen, N. Pryds, J. E. Kleibeuker, G. Koster, J. Sun, E. Stamate, B. Shen, G. Rijnders, S. Linderoth, *Nano Lett.* **2011**, *11*, 3774.
[9] G. Herranz, F. Sánchez, N. Dix, M. Scigaj, J. Fontcuberta, *Sci. Rep.* **2012**, *2*, 758.
[10] Z. Q. Liu, C. J. Li, W. M. Lü, X. H. Huang, Z. Huang, S. W. Zeng, X. P. Qiu, L. S. Huang, A. Annadi, J. S. Chen, J. M. D. Coey, T. Venkatesan, Ariando, *Phys. Rev. X* **2013**, *3*, 021010.
[11] K. Ueno, S. Nakamura, H. Shimotani, A. Ohtomo, N. Kimura, T. Nojima, H. Aoki, Y. Iwasa, M. Kawasaki, *Nat. Mater.* **2008**, *7*, 855.
[12] W. Meevasana, P. D. C. King, R. H. He, S. Mo, M. Hashimoto, A. Tamai, P. Songsiriritthigul, F. Baumberger, Z. Shen, *Nat. Mater.* **2011**, *10*, 114.
[13] S. McKeown Walker, A. de la Torre, F. Y. Bruno, A. Tamai, T. K. Kim, M. Hoesch, M. Shi, M. S. Bahramy, P. D. C. King, F. Baumberger, *Phys. Rev. Lett.* **2014**, *113*, 177601.
[14] Z. Wang, Z. Zhong, X. Hao, S. Gerhold, B. Stöger, M. Schmid, J. Sánchez-Barriga, A. Varykhalov, C. Franchini, K. Held, U. Diebold, *Proc. Natl. Acad. Sci. USA* **2014**, *111*, 3933.
[15] A. Fête, C. Cancellieri, D. Li, D. Stornaiuolo, A. D. Caviglia, S. Gariglio, J.-M. Triscone, *Appl. Phys. Lett.* **2015**, *106*, 051604.
[16] Y. Lee, C. Clement, J. Hellerstedt, J. Kinney, L. Kinnischtzke, X. Leng, S. D. Snyder, A. M. Goldman, *Phys. Rev. Lett.* **2011**, *106*, 136809.
[17] A. Joshua, S. Pecker, J. Ruhman, E. Altman, S. Ilani, *Nat. Commun.* **2012**, *3*, 1129.
[18] M. Stengel, *Phys. Rev. Lett.* **2011**, *106*, 136803.
[19] M. Salluzzo, J. C. Cezar, N. B. Brookes, V. Bisogni, G. M. De Luca, C. Richter, S. Thiel, J. Mannhart, M. Huijben, A. Brinkman, G. Rijnders, G. Ghiringhelli, *Phys. Rev. Lett.* **2009**, *102*, 166804.
[20] A. D. Caviglia, S. Gariglio, C. Cancellieri, B. Sacépé, A. Fête, N. Reyren, M. Gabay, A. F. Morpurgo, J.-M. Triscone, *Phys. Rev. Lett.* **2010**, *105*, 236802.
[21] A. Fête, S. Gariglio, A. D. Caviglia, J.-M. Triscone, M. Gabay, *Phys. Rev. B* **2012**, *86*, 201105.
[22] A. McCollam, S. Wenderich, M. K. Kruize, V. K. Guduru, H. J. A. Molegraaf, M. Huijben, G. Koster, D. H. A. Blank, G. Rijnders, A. Brinkman, H. Hilgenkamp, U. Zeitler, J. C. Maan, *APL Mater.* **2014**, *2*, 022102.
[23] G. Berner, M. Sing, H. Fujiwara, A. Yasui, Y. Saitoh, A. Yamasaki, Y. Nishitani, A. Sekiyama, N. Pavlenko, T. Kopp, C. Richter, J. Mannhart, S. Suga, R. Claessen, *Phys. Rev. Lett.* **2013**, *110*, 247601.
[24] C. Cancellieri, M. L. Reinle-Schmitt, M. Kobayashi, V. N. Strocov, P. R. Willmott, D. Fontaine, P. Ghosez, A. Filippetti, P. Delugas, V. Fiorentini, *Phys. Rev. B* **2014**, *89*, 121412.
[25] A. F. Santander-Syro, O. Copie, T. Kondo, F. Fortuna, S. Pailhès, R. Weht, X. G. Qiu, F. Bertran, A. Nicolaou, A. Taleb-Ibrahimi, P. Le Fèvre, G. Herranz, M. Bibes, N. Reyren, Y. Apertet, P. Lecoeur, A. Barthélémy, M. J. Rozenberg, *Nature* **2011**, *469*, 189.
[26] P. D. C. King, S. McKeown Walker, A. Tamai, A. de la Torre, T. Eknapakul, P. Buaphet, S.-K. Mo, W. Meevasana, M. S. Bahramy, F. Baumberger, *Nat. Commun.* **2014**, *5*, 3414.
[27] H. O. Jeschke, J. Shen, R. Valenti, *New J. Phys.* **2015**, *17*, 023034.
[28] C. Lin, A. A. Demkov, *Phys. Rev. Lett.* **2013**, *111*, 217601.
[29] F. Lechermann, L. Boehnke, D. Grieger, C. Piefke, *Phys. Rev. B* **2014**, *90*, 085125.
[30] M. Sing, G. Berner, K. Goß, A. Müller, A. Ruff, A. Wetscherek, S. Thiel, J. Mannhart, S. A. Pauli, C. W. Schneider, P. R. Willmott, M. Gorgoi, F. Schäfers, R. Claessen, *Phys. Rev. Lett.* **2009**, *102*, 176805.
[31] E. Slooten, Z. Zhong, H. Molegraaf, P. Eerkes, S. de Jong, F. Massee, E. van Heumen, M. Kruize, S. Wenderich, J. Kleibeuker, M. Gorgoi, H. Hilgenkamp, A. Brinkman, M. Huijben, G. Rijnders, D. Blank, G. Koster, P. Kelly, M. Golden, *Phys. Rev. B* **2013**, *87*, 085128.
[32] Y. Z. Chen, N. Bovet, T. Kasama, W. W. Gao, S. Yazdi, C. Ma, N. Pryds, S. Linderoth, *Adv. Mater.* **2014**, *26*, 1462.
[33] M. Knotek, P. Feibelman, *Phys. Rev. Lett.* **1978**, *40*, 964.
[34] M. L. Knotek, *Phys. Today* **1984**, *37*, 24.
[35] O. Dulub, M. Batzilln, S. Solovev, E. Loginova, A. Alchagirov, T. E. Madey, U. Diebold, *Science* **2007**, *317*, 1052.
[36] S. Moser, L. Moreschini, J. Jaćimović, O. S. Barišić, H. Berger, A. Magrez, Y. J. Chang, K. S. Kim, A. Bostwick, E. Rotenberg, L. Forró, M. Grioni, *Phys. Rev. Lett.* **2013**, *110*, 196403.